







Enhancing Extreme Precipitation Predictions With Dynamical Downscaling: A Convection-Permitting Modeling Study in Texas and Oklahoma

Hsin-I. Chang¹ , Yoshimitsu Chikamoto² , Simon S.-Y. Wang² , Christopher L. Castro¹, Matthew D. LaPlante^{2,3} , C. Bayu Rianto¹ , Xingying Huang⁴ , and Patrick Bunn¹

¹Department of Hydrology and Atmospheric Sciences, University of Arizona, Tucson, AZ, USA, ²Department of Plants, Soils and Climate, Utah State University, Logan, UT, USA, ³Department of Journalism and Communication, Utah State University, Logan, UT, USA, ⁴National Center for Atmospheric Research, Boulder, CO, USA

Key Points:

- Dynamical downscaling could improve the performance of fully coupled low resolution climate model in simulating climate conditions over land
- Consistent improvements from convective-permitting modeling in the depiction of precipitation for extreme Texas flood and drought years
- Improved regional circulation pattern depiction, combined with convective-permitting modeling, leads to enhanced precipitation simulation

Supporting Information:

Supporting Information may be found in the online version of this article.

Correspondence to:

H.-I. Chang,
hchang05@arizona.edu

Citation:

Chang, H.-I., Chikamoto, Y., Wang, S. S.-Y., Castro, C. L., LaPlante, M. D., Rianto, C. B., et al. (2024). Enhancing extreme precipitation predictions with dynamical downscaling: A convection-permitting modeling study in Texas and Oklahoma. *Journal of Geophysical Research: Atmospheres*, 129, e2023JD038765. <https://doi.org/10.1029/2023JD038765>

Received 23 FEB 2023
Accepted 23 FEB 2024

Author Contributions:

Conceptualization: Hsin-I. Chang, Yoshimitsu Chikamoto, Simon S.-Y. Wang, Christopher L. Castro
Data curation: Hsin-I. Chang, Yoshimitsu Chikamoto, Patrick Bunn
Formal analysis: Hsin-I. Chang, Yoshimitsu Chikamoto, C. Bayu Rianto
Funding acquisition: Simon S.-Y. Wang
Investigation: Hsin-I. Chang, Yoshimitsu Chikamoto
Methodology: Hsin-I. Chang, Yoshimitsu Chikamoto, Christopher L. Castro
Project administration: Simon S.-Y. Wang
Resources: Hsin-I. Chang, Yoshimitsu Chikamoto

Abstract Precipitation in the Southern Plains of the United States is relatively well depicted by the Community Earth System Model (CESM). However, despite its ability to capture seasonal mean precipitation anomalies, CESM consistently underestimates extreme pluvial and drought events, rendering it an insufficient tool for extending simulation lead times for exceptional events, such as the abnormally dry May 2011, which helped drive Texas into its worst period of drought in more than a century, and the abnormally wet May 2015, which led to widespread flooding in that state. Ensemble-based regional climate experiments are completed for the two extreme years using Weather Research and Forecasting model (WRF) and downscaled from CESM. WRF simulations are at convection-permitting grid resolution for improved physical representation of simulated precipitation over the Southern Great Plains. By integrating convection-permitting models (CPMs) into each individual member of a CESM ocean data assimilation ensemble, this study demonstrates that high-resolution dynamical downscaling can improve model skillfulness at capturing these two events and is thus a potentially useful tool for forecasting extremely high and extremely low precipitation events at subseasonal or even seasonal lead times.

Plain Language Summary The Community Earth System Model (CESM) has reasonable climatological representation over the Southern Plains region of the United States, but it is still a challenge for CESM to capture the extreme events like severe floods and drought. In this study, we applied a regional climate modeling approach onto CESM at a model resolution capable of resolving convection for selected record-breaking wet and dry years in Texas. Results indicate our modeling approach can improve CESM's capability to simulate both wet and dry extremes and the modeling system skill is reasonable using CESM simulations initialized weeks before the events' occurrence. Different sources of upper atmospheric zonal winds may lead to abnormally wet or dry seasonal precipitation in Texas.

1. Introduction

Global convective precipitation has exhibited a significant increase in intensity during the past 30 years owing to two factors related to climate warming. First, increases in atmospheric moisture and instability have created a more thermodynamically favorable convective environment and more organized severe storms (e.g., Holloway & Neelin, 2009; Luong et al., 2017; Trenberth, 2011). Second, amplified mid-latitude atmospheric circulation has led to more persistent blocking patterns (Coumou et al., 2014). These factors are particularly at play during the boreal warm season, and have occurred in conjunction with a strengthening of atmospheric teleconnections (e.g., Chang et al., 2015; Coumou et al., 2014; Wang et al., 2014). It has also been demonstrated that persistent standing wave patterns have caused more intensified flooding and drought episodes within the continental United States in recent decades (e.g., Crosci-Maspoli et al., 2007; Francis & Vavrus, 2012; Schubert et al., 2011; Screen & Simmonds, 2013; Wang et al., 2013).

Precipitation variability over the Southern Plains of the United States (encompassing Texas and Oklahoma) is influenced by two climatic features, namely the peak rainy season that occurs in May associated with a “spring trough” (Kelly et al., 1978; Nigam & Ruiz-Barradas, 2006; Roads et al., 1994) and its relatively persistent response to the teleconnection of the El Niño-Southern Oscillation (Lee et al., 2014). Ghebreyesus and Sharif (2021) examined the Texas precipitation climatology between 2002 and 2019, finding a significant

Software: Hsin-I. Chang, Yoshimitsu Chikamoto, C. Bayu Risanto, Xingying Huang
Supervision: Simon S.-Y. Wang, Christopher L. Castro
Validation: Hsin-I. Chang, Yoshimitsu Chikamoto
Visualization: Hsin-I. Chang, C. Bayu Risanto
Writing – original draft: Hsin-I. Chang, Yoshimitsu Chikamoto
Writing – review & editing: Hsin-I. Chang, Yoshimitsu Chikamoto, Simon S.-Y. Wang, Christopher L. Castro, Matthew D. LaPlante

increase in precipitation frequency occurred after the 2011–2012 drought, especially during summertime and over the northern part of the Gulf Coast. September was observed to be the wettest month in Texas and April was the driest. In May 2015, the development of the spring trough coincided with the growing phase of a strong El Niño leading to a semi-stationary, synoptic-scale trough that initiated consecutive rainstorms passing through Texas and Oklahoma over a duration of 20+ days, resulting in a devastating flood (Wang et al., 2015). Diallo et al. (2019) identified the low-level jet stream originating from the Gulf of Mexico as the source of Southern Plains precipitation during the same 2015 flood period. Despite a general agreement that the low-level jet stream plays a crucial role in the precipitation extremes of May in the Southern Plains (Diallo et al., 2019; Higgins et al., 1997; Wang & Chen, 2009; Wang et al., 2015), the impact of the upper-level jet stream on precipitation remains uncertain.

Warm-season precipitation in the Southern Plains, due to its pronounced coupling with large-scale drivers, is relatively well depicted by the Community Earth System Model (CESM) in historical simulations (Wang et al., 2015; Yoon & Leung, 2015). Chikamoto, Johnson, et al. (2020) showed that the precipitation simulation of the western United States (including the Southern Plains) could be improved through ocean data assimilation (ODA). This computationally efficient approach of combining the coarse-resolution but fully coupled CESM with ODA demonstrated reasonable performance in simulating seasonal-to-decadal Earth system variability (Chikamoto, Johnson, et al., 2020; Johnson et al., 2018, 2020; Stuijvenolt-Allen et al., 2021). By explicitly forecasting the temporal evolution of ocean conditions, this integrated method has been shown to be highly effective in capturing and predicting various climatic phenomena, such as Atlantic Meridional Overturning Circulation, Pacific Decadal Oscillation, and North Pacific Gyre Oscillation (Chikamoto et al., 2017, 2019, 2020a). Despite its ability to capture the seasonal mean precipitation anomaly, the CESM simulations with ODA (CESM ODA here after) underestimated the extreme precipitation and could not resolve convective rainfall where it occurred due to coarse horizontal resolution. Use of regional convection-permitting models (CPMs) may be a way to address this deficiency to better resolve convective storms (Castro et al., 2012; Meredith et al., 2015). CPMs more reasonably represent precipitation extremes owing to their better representation of the local storm dynamics (Fosser et al., 2020) and topography influences (Vanden Broucke et al., 2019). CPMs have been studied for their potential to improve predictability of extreme rainfall and diurnally evolved storms in both weather forecast and subseasonal forecast time scales (Capecchi, 2021; Nielsen & Schumacher, 2016; Risanto et al., 2019). The use of CPMs in downscaling seasonal and longer-term predictions has also been explored, with mixed success in predictability enhancement depending on the locations and storm types (Prein et al., 2015; Qing & Wang, 2021). Studies using CPMs to examine future climate projections have found an overall improvement in the representation of convective storms and associated changes in seasonal mean precipitation and occurrence (e.g., Chang et al., 2015; Kendon et al., 2017). In addition to model spatial resolution, RCM's capability in simulating regional convections is also sensitive to the model physical parameterization and land surface processes (e.g., Bukovsky & Karoly, 2011). For the Great Plains convective activities, CPMs specifically have improved capability in capturing the diurnal cycles and the low-level jet moisture transport (Scaff et al., 2020; Sun, Xue, et al., 2016).

In this study, to combine the strength of CESM ODA, which is skillful at capturing large-scale features, with more accurate representations of fine-scale extreme precipitation, Weather Research and Forecasting model (WRF) downscaled CESM ODA ensemble experiments are used to simulate 2 years where extreme conditions were experienced in the Southern Plains in late spring. We examine the WRF ensemble simulations forced by the CESM ODA outputs as the lateral boundary conditions for the extreme flooding that occurred in Texas in May 2015 and the onset of a record drought in the same region in May 2011. Large-scale circulation signals associated with the flood and drought periods are also evaluated.

2. Materials and Methodology

2.1. Gridded Precipitation Observation Data Sets

For the WRF simulation verification and evaluation, we compared WRF performance with multiple observation data sets. One of the observation baselines used is the National Center for Environmental Prediction (NCEP) Stage-IV precipitation data set. The 4-km resolution with the 6-hourly temporal resolution data set comprises radar and gauge measurements that are quality controlled by 12 River Forecast Centers (Lin & Mitchell, 2005). It has been used as ground truth for verification of regional climate model forecasts at meso-beta and meso-gamma

WRF-CPM Ensemble Domains

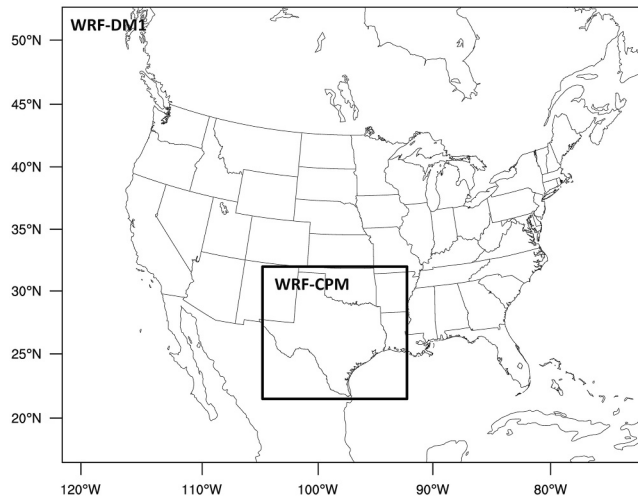


Figure 1. WRF simulation domains at 12 and 4 km resolutions.

resolutions in the United States (e.g., Prein et al., 2020; Sun, Riva, & Dittmar, 2016). Another observed-based precipitation source is provided by the Global Precipitation Climatology Center (GPCC, Schneider et al., 2017). The 0.25° resolution global mean land surface precipitation data set used in this study is generated based on quality-controlled in-situ measurements. GPCC precipitation is also commonly used for numerical model validation, hydroclimate studies and impact assessments at global and regional scale (e.g., Karmalkar et al., 2011; Sun et al., 2018).

2.2. Weather Research and Forecasting Model

For the convective-permitting model, we use the Advanced Research version of the Weather Research and Forecasting model (WRF-ARW; Powers et al., 2017; Skamarock et al., 2008) version 3.8 with two nested domains at 12 and 4 km model resolution. The outer domain covers the entire continental U.S. (WRF-DM1), and the inner domain covers the majority of Texas (WRF-CPM) (Figure 1). Specific model physical configuration follows the WRF simulation design in Risanto et al. (2019). The model's inner domain has a convective-permitting horizontal grid spacing, in which the WRF-ARW explicitly resolves convection at the meso- γ scale (1–4 km) without engaging any convective parameterization scheme. Two sets of WRF simu-

lations are completed for both the extreme wet year (2015) and extreme dry year (2011). Each WRF simulation is initialized in March and ends in June. The majority of the statistical analyses presented in the manuscript are from its 4km-resolution domain.

2.3. CESM With Ocean Data Assimilation (ODA)

We adopted the coarse-resolution version of the fully coupled climate model CESM 1.0.6 (Chikamoto et al., 2019; Shields et al., 2012). Based on this model, we obtained the boundary climate forcing for the WRF-ARW from the ocean data assimilation run. The CESM's atmospheric and land components consist of T31 spectral resolution at 26 atmospheric and 15 soil levels. The T31 resolution CESM has been scientifically validated and is computationally more efficient for this purpose compared to other higher resolution CESM products. Ocean and sea-ice components correspond to a horizontal curvature grid with a displaced North Pole ($\sim 3^\circ$ horizontal grid but 1° latitude grid near the equator) and 60 vertical levels in the ocean (Shields et al., 2012). For the ocean data assimilation, we assimilated the 3-dimensional observed ocean temperature and salinity anomalies into the ocean component of CESM while prescribing the natural and anthropogenic radiative forcings (i.e., greenhouse gas and aerosol concentrations, solar cycle variations, and major volcanic eruptions). The assimilated observed ocean data originates from the ECMWF ocean reanalysis from 1958 to 2016 (Balmaseda et al., 2013). These data are linearly interpolated from daily anomalies and added as forcing into the model's temperature and salinity tendency equations using an incremental analysis update scheme (Bloom et al., 1996; Huang et al., 2002). The radiative forcings use the pre-2005 record and the IPCC RCP4.5 post-2005 emissions scenario.

We conducted the ocean data assimilation (ODA) run for 1958–2015 using 10 CESM ensemble members prescribed by the same observed ocean data and radiative forcings but with different initial conditions set on 1 January 1958. We applied an anomaly assimilation technique (i.e., assimilating the observed anomaly with the model climatology), which can minimize the artificial influence of model drift, initialization shocks, and energy imbalances in large-scale atmosphere-ocean interactions (Chikamoto et al., 2019). Details of the basic model performance in this system are referred to in Chikamoto et al. (2017, 2019, 2020a). Because of our experimental setting, we can assume that the atmospheric variability simulated by the ensemble mean of the CESM ODA run corresponds to the potential predictability if the model could perfectly predict ocean variability. Each member of the CESM ODA ensembles was dynamically downscaled using WRF for two climatologically severe springtime anomalies in Texas as described above: the flood year of 2015 and the drought year of 2011. We completed the downscaling simulation for all CESM ODA ensemble members and evaluated the simulations using a verification matrix, which is explained next.

2.4. Model Simulation Verification Matrix

Model simulation verification analyses were performed using the categorical statistics methods based on the contingency table; this was to preserve the characteristics of individual ensemble members without doing the ensemble averaging. WRF ensemble skill was evaluated against gridded observations. In this paper, we mainly examined the skill for total monthly precipitation from WRF and CESM ODA ensembles using the following process: each of the observation grids was compared against the neighboring WRF grid points at a certain size (a 25×25 grid at 4 km resolution, equivalent to a 100×100 km area). Verification results at each grid point were then assigned as one of the following: hit, miss, false alarm or correct negative. We then applied the four assigned verification results to the 2×2 forecast contingency table. Several precipitation thresholds are selected to examine the simulation capability of WRF during wet and dry years. Specific thresholds will be presented in the results section.

Several statistical analysis methods based on the contingency table are used for this study: Probability of Detection (POD), False Alarm Rate (FAR) and Relative Operating Characteristics (ROC). POD and FAR are used to determine the simulation capability (Wilks, 2006), following the evaluation thresholds and size detailed above. Both POD and FAR values are between 0 and 1. POD value closer to one indicates higher modeling skill. On the other hand, FAR value closer to 1 means a higher false alarm rate and lower modeling skill. The ROC is used to evaluate the ability of the WRF forecast probability of precipitation (or any other variables) beyond certain thresholds respective to observations. The ROC curve classifies the simulation results into hits or misses based on the observations and is plotted as a true positive rate in the y -axis and false positive rate in the x -axis. Area under the curve (AUC) indicates the model skill: An AUC value closer to one indicates good skill while an AUC that is less than 0.5 is indicative of no skill. The ROC analysis metric includes evaluations from individual ensemble members and is shown as a combined verification metric. ROC can also be considered as a measure of modeling confidence and reliability for ensemble analysis (Harvey et al., 1992).

3. Results

3.1. Precipitation Simulations for Both Extreme Flood and Drought Years Through WRF Ensemble Downscaling

To evaluate the value-added through convective-permitting modeling in simulating convective extremes, we first evaluated May precipitation for the 2015 flood year and the 2011 drought year. The observational Global Precipitation Climatology Center (GPCC, Schneider, 2017) precipitation indicated widespread, abnormally high precipitation in May 2015 over Texas (Figure 2a), a result of a series of convective storms embedded in the semi-stationary baroclinic circulation features (Wang et al., 2015). The CESM ODA ensemble mean shows a reasonable performance in simulating large amounts of precipitation over Texas (Figure 2b). However, individual ensemble members have various precipitation simulation skills, the extreme values were either displaced or missing. WRF ensemble means from both the outer domain (WRF-DM1 non-CPM) and inner nested WRF-CPM domain (Figures 2c and 2d) can better resolve precipitation patterns as compared to driving CESM ODA, suggesting that grid spacing does have an impact. Figure 2c shows the WRF ensemble mean for the flooding year and appears to depict the extreme precipitation more realistically than the CESM ODA output, especially near the coastal region near the Gulf of Mexico. The WRF ensemble wet bias over the southeastern U.S. is a common model bias (Castro et al., 2012). Each WRF ensemble has various skill in capturing the convective activity of May 2015. The WRF ensemble mean (Figures 2c and 2d) still presents some skill in representing the extreme precipitation, suggesting a positive impact of grid spacing (More in-depth statistical analyses are presented in the following sections). Correspondingly for the abnormally dry month of May 2011 (Figures 2e–2h), the CESM ODA ensemble mean produced relatively low precipitation over most of Texas than WRF (Figure 2f), except in the Texas Panhandle and North Texas. Notably, the over-predicted May 2011 precipitation is reduced by WRF downscaling (Figures 2g and 2h). When evaluating the monthly precipitation from individual ensemble members, some CESM ODA members produced much wetter conditions for the drought year. This pattern of overprediction was remedied on the WRF domain downscaled from CESM ODA (individual members not shown). These results reflect the fact that the raw global model/CESM ensemble generally fails to capture precipitation extremes. However, when CPM dynamical downscaling is applied to the same CESM ODA ensemble, WRF substantially improved the simulation of extreme precipitation. The improvement applies to abnormally dry seasons like May 2011 as well as abnormally wet periods like May 2015. Given that the CESM ODA output is an important step

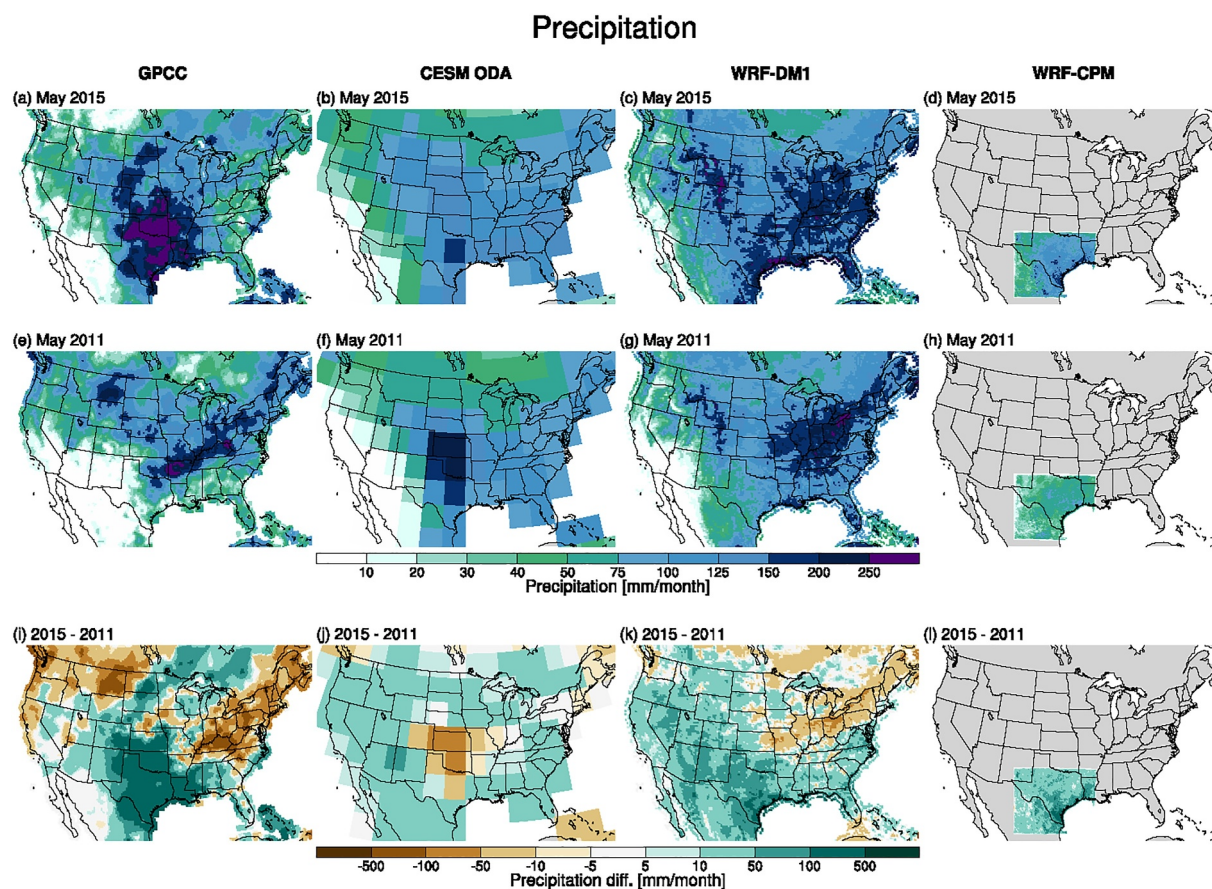


Figure 2. May precipitation comparison for 2015 (Figures 2a–2d), 2011 (Figures 2e–2h) and difference plots (Figures 2i–2l). The first column is observations provided by GPCC, the second column is from the CESM ODA ensemble mean, and the third and fourth columns are ensemble means from the WRF outer and inner domains.

toward seasonal forecasting, this improvement in modeled precipitation via WRF may potentially translate to an enhanced modeling capability.

Various precipitation performances are also found for the May 2015 flood year from the WRF-CPM ensembles (Figure S6 in Supporting Information S1). Overall, during that extremely wet season, the WRF-CPM members generated higher precipitation amounts, which were closer to observations than the parent CESM ODA outputs. However, these simulation improvements are not uniform among different ensemble members. The ensuing analyses will explore the quantitative skill scores and the dynamical connection between the simulated precipitation and associated circulation fields.

3.2. Model Simulation Verification

Monthly precipitation analyses for the individual WRF ensemble members show large precipitation variability within the ensemble is a function of the CESM ODA initial and boundary forcing. Especially during months with the greatest amounts of precipitation, such as May 2015, the precipitation simulated by WRF is highly variable in timing, location, and magnitude. We designed verification metrics specifically to maintain precipitation characteristics from individual ensemble members and computed the skill analysis considering all ensemble members. To quantify the performance difference that occurs when using the WRF, we evaluated the model simulation capability of monthly precipitation from the raw CESM ODA results and WRF ensembles. The precipitation POD was evaluated for various precipitation thresholds to identify the potential improvement using high-resolution WRF for both drought and wet periods. POD was calculated using the contingency table-based analysis to compare modeled forecasts against observations, such as POD from WRF (as compared to observation) and POD from CESM ODA (against observation). We first calculated the PODs of WRF and driving CESM ODA to depict the potential changes in WRF skill from CESM ODA (Figure 3). During the 2015 flood year, the driving CESM

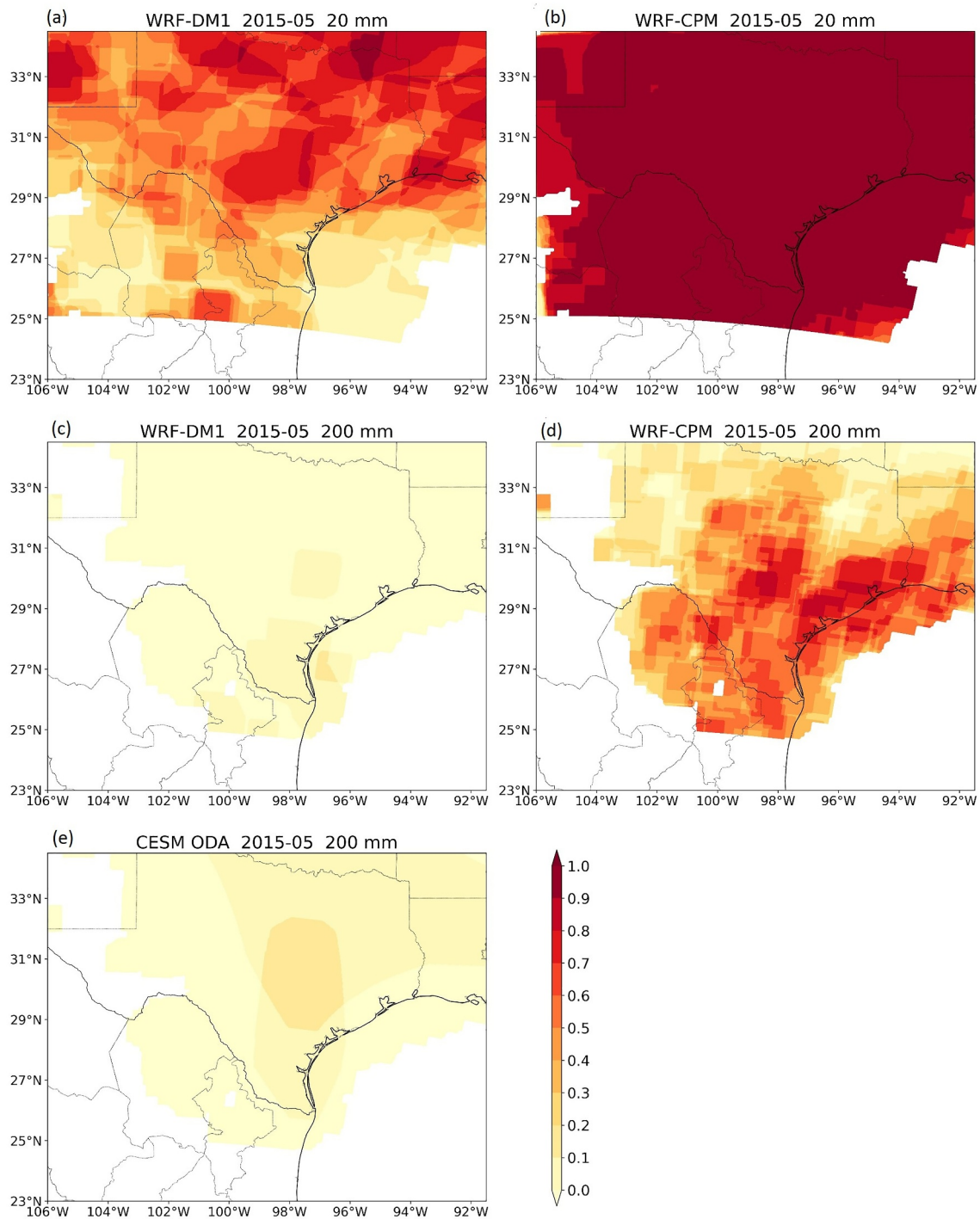


Figure 3. Probability of Detection score for 2015 May precipitation: (a) WRF-DM1 at 20 mm threshold, (b) WRF-CPM at 20 mm threshold, (c) WRF-DM1 at 200 mm threshold, (d) WRF-CPM at 200 mm threshold, (e) CESM ODA at 200 mm threshold. The POD analysis compares precipitation values between WRF simulations with Stage IV observation.

ODA presented an overall low probability to capture the extreme precipitation threshold (200 mm) for the entire study domain (Figure 3e). Significant POD improvements are found in the WRF simulation (Figure 3b). The area of POD improvement corresponds to most extreme precipitation from Stage IV data.

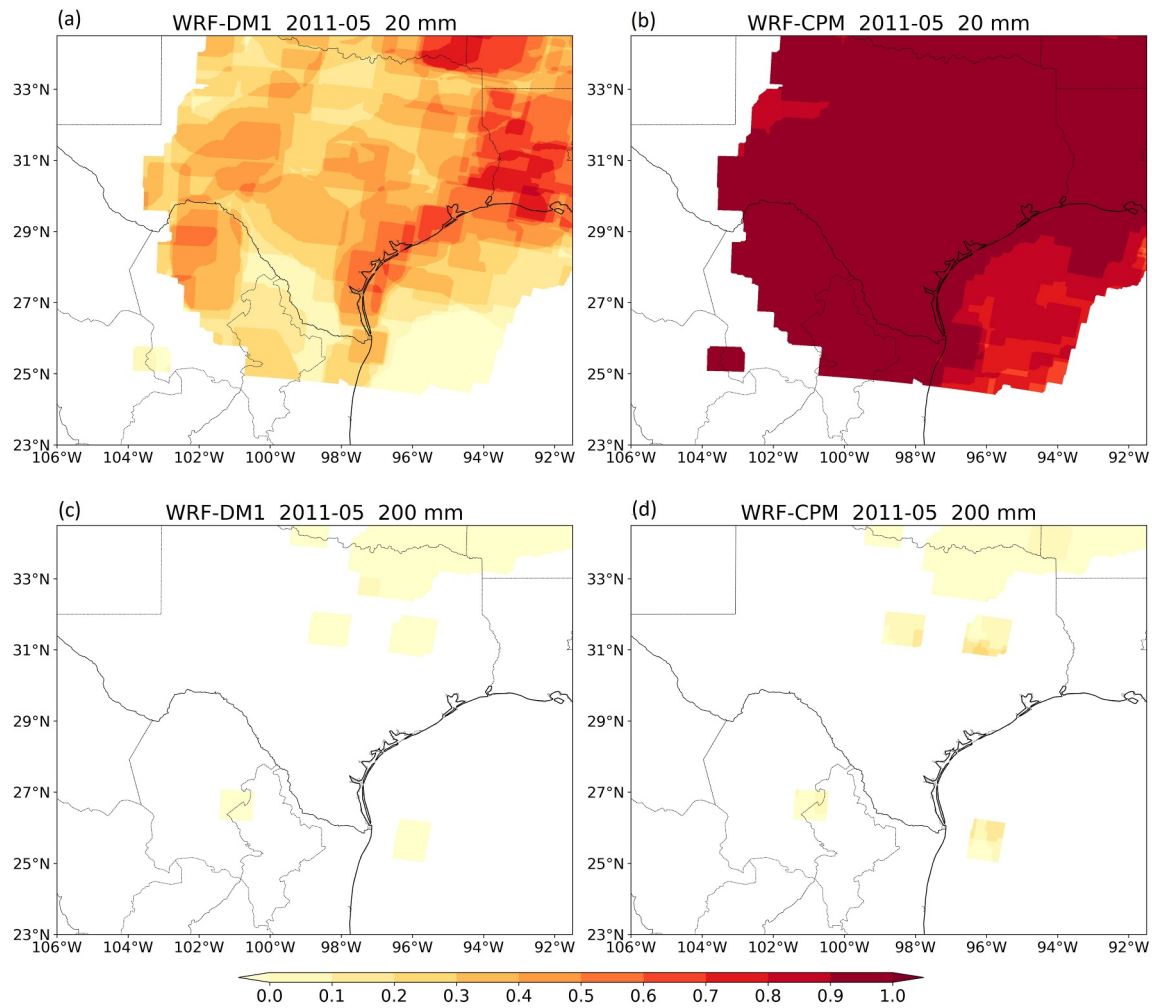


Figure 4. Probability of Detection score for 2011 May precipitation: (a) WRF-DM1 at 20 mm threshold, (b) WRF-CPM at 20 mm threshold, (c) WRF-DM1 at 200 mm threshold, (d) WRF-CPM at 200 mm threshold. The POD analysis compares precipitation values between WRF simulations with Stage IV observation.

Next, we evaluated WRF model sensitivity for capturing different precipitation thresholds. POD of the WRF-CPM domain ensembles has a good probability of precipitation detection across various precipitation thresholds (Figures 3b and 3d), compared to the WRF-DM1 outer domain simulations, and is also valid in the dry period. The 2011 drought year POD analysis is shown in Figure 4. At the 20 mm threshold, the probability of detection is significantly higher in the WRF-CPM domain than the coarser WRF-DM1 domain (Figures 4a and 4b). For comparison, the 200 mm threshold POD for 2011 is also shown (Figures 4c and 4d), both WRF domains accurately simulated the dry period with near zero POD values. WRF-CPM POD tends to increase with a higher precipitation threshold, indicating a better ability to represent precipitation extremes. The largest precipitation model simulation improvement was observed at extreme precipitation thresholds. CESM ODA and WRF-CPM analyses at a 20 mm precipitation threshold have similar POD values across the domain (figure not shown), while WRF-CPM substantially improves the May 2015 POD from CESM ODA at a 200 mm threshold (Figure 3d vs. Figure 3e). Since the 2015 WRF ensemble simulations began in March and flood and drought are affected by the antecedent land surface and soil conditions, we also examined the precipitation forecast skill in April 2015 prior to the period of most active convective precipitation. As was the case in the May 2015 analysis, POD for April exhibits reasonable skill at a lower precipitation threshold and was significantly improved by WRF-CPM (Figure S1 in Supporting Information S1). The spring months leading to May 2015 were consistently recording above-average precipitation over Texas; March 2015 was the fourth wettest and April 2015 was the fifth wettest on record. However, the value-added from WRF-CPM is less pronounced at the extreme precipitation threshold in the April POD analysis (Figure S1 in Supporting Information S1). Overall, the POD analyses demonstrated that

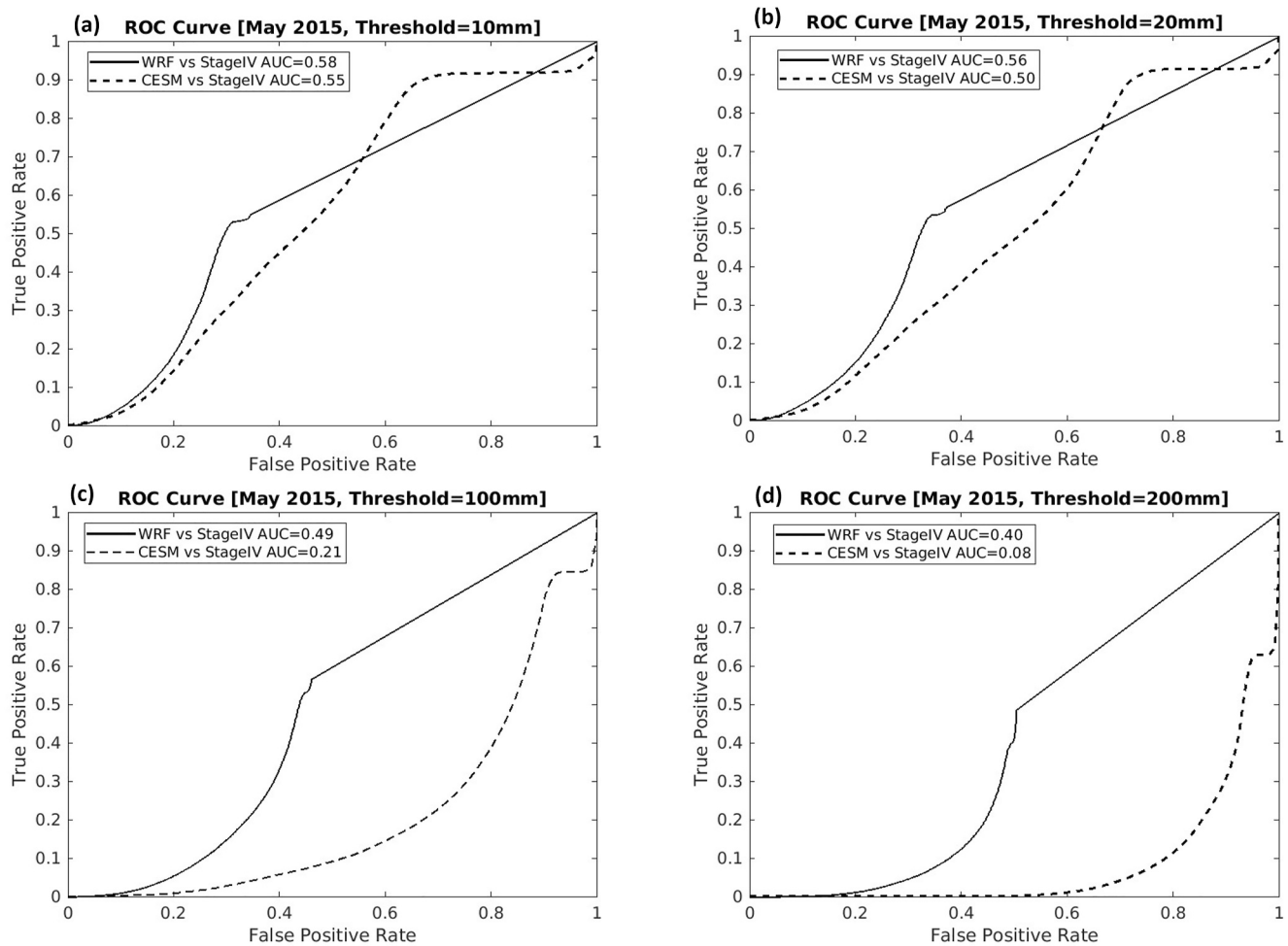


Figure 5. May 2015 ROC analysis for precipitation thresholds at 10, 20, 100 and 200 mm.

WRF-CPM provides improvement in simulating precipitation extremes, especially during the months with most extreme precipitation.

We also evaluated the model simulation probability by classifying the monthly precipitation hit and miss ratio against observations. WRF-CPM significantly improved the probability skill (ROC) at different precipitation thresholds. The ROC is generally used as a function to evaluate the forecast probability of numerical modeling ensembles, against gridded observations, at the gridpoint level. All modeling ensemble data sets used are regridded in alignment with observation data sets. We are able to preserve the characteristics from individual ensemble simulations by performing a grid-by-grid ROC analysis for each of the 10 ensemble members against observations. Similar to the POD analyses, ROC analyses are also performed at various precipitation thresholds. For the May precipitation in the 2015 flood year, WRF-CPM ensembles and the driving CESM ODA ensembles have similar skill at 10 and 20 mm thresholds, given the similar ROC patterns and AUC values (Figure 5, left 2 panels). Both CESM ODA and WRF-CPM have some skill to capture the 10 and 20 mm precipitation thresholds with AUC values >0.5 . As described in model simulation verification matrix, when AUC value is greater than 0.5, the forecast is considered skillful. More substantial differences in the ROC analyses can be found at higher precipitation thresholds (Figure 5 right 2 panels). CESM ODA skill significantly decreased at the 100 and 200 mm thresholds, but WRF-CPM ensembles consistently exhibited larger skill from across all of the precipitation thresholds. There is a lesser number of grid points at 10 and 20 mm precipitation from CPM, and more grid points at the higher thresholds, leading to significant improvements in probability at those levels. The months before May 2015 also recorded higher than normal precipitation, and the WRF-CPM skill these months has some level of improvements (Figure S2 in Supporting Information S1). For the May 2011 climatology, both WRF-CPM and

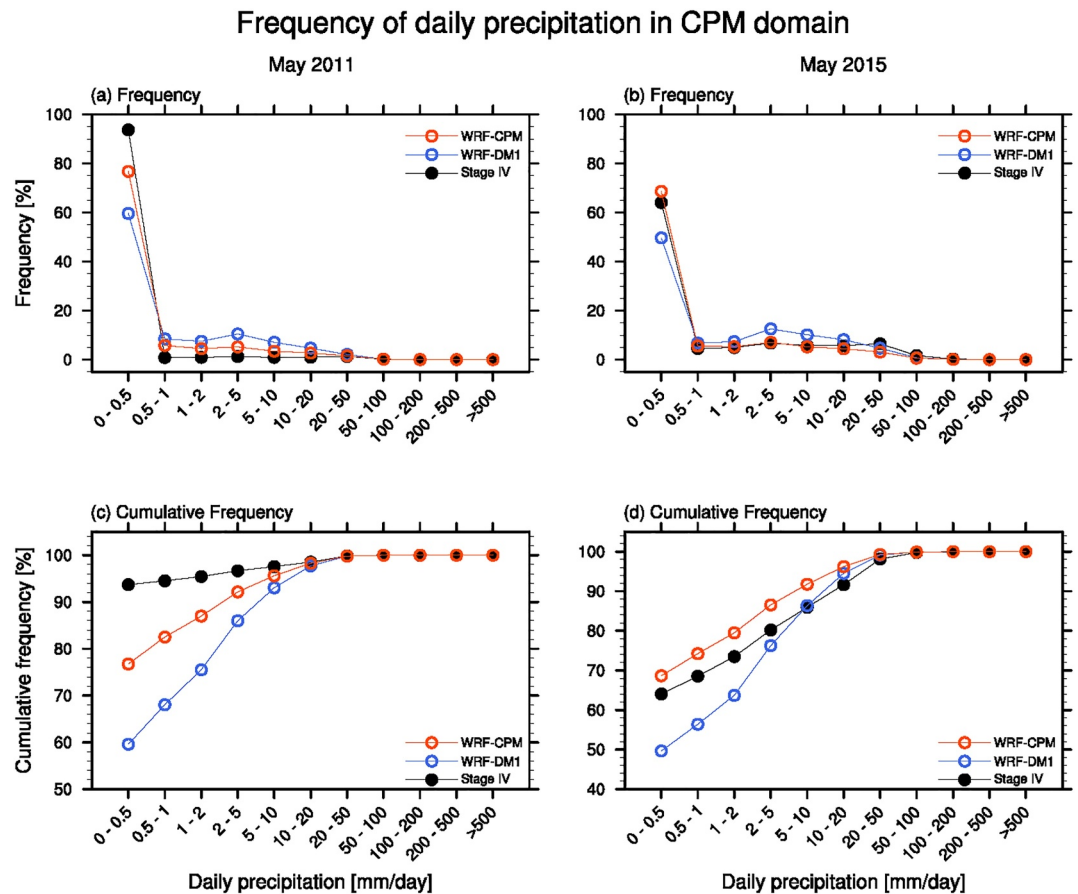


Figure 6. Frequency and cumulative frequency of precipitation occurrence (top and bottom row) with respect to different precipitation thresholds. Red: WRF-CPM, blue: WRF-DM1 and black: Stage IV.

CESM ODA have jagged ROC curves due to a limited number of observed precipitation points for verification (Figure S3 in Supporting Information S1). CESM ODA ROC analyses consistently show no forecast skill in simulating high precipitation thresholds, and improved skills are seen from WRF-CPM ensemble.

We further analyzed the frequency of occurrence of precipitation thresholds using a logarithm scale (Figure 6, upper panel). Generally, WRF-CPM (red) exhibits superior performance in simulating the probability distribution of daily precipitation observed in Stage IV (black), outdoing WRF-DM1 (blue), except for the 10–50 mm/day category in May 2015. WRF-DM1 shows wet biases, leading to underestimations of low precipitation conditions ($0 < \text{precipitation} < 0.5$ mm/day category) and overestimations of medium precipitation ($1 < \text{precipitation} < 10$ mm/day category). This leads to wet biases in WRF-DM1's monthly precipitation. The cumulative frequency plot emphasizes CPM's improvement, particularly for low precipitation ranges of less than 10 mm/day in May 2011 (lower left panel) and less than 2 mm/day in May 2015 (lower right panel). Consistent with these findings, WRF-DM1 fails to capture the precipitation-free region around New Mexico and western Texas during May 2011 (Figures 2e and 2g). Such model biases could be ameliorated by employing the convective-permitting model.

3.3. Diagnostics for the Large-Scale Circulation

This section evaluates how large-scale atmospheric circulations affect Texas precipitation extremes in the CESM ODA output. To highlight the jet stream impact, we made maps of zonal winds at 250 hPa and land precipitation in May 2011 and May 2015 for observation-based products and the ensemble means of CEMS ODA and WRF-DM1 simulations (Figure 7). In May 2011, stronger U250 areas (>20 m/s) extend from the North Pacific to the Southwest (Figure 7a). This wind pattern is preferential for the transport of dry air from the polar region toward Texas through an active subpolar jet. As a result, lower precipitation area was extended into the Southwest,

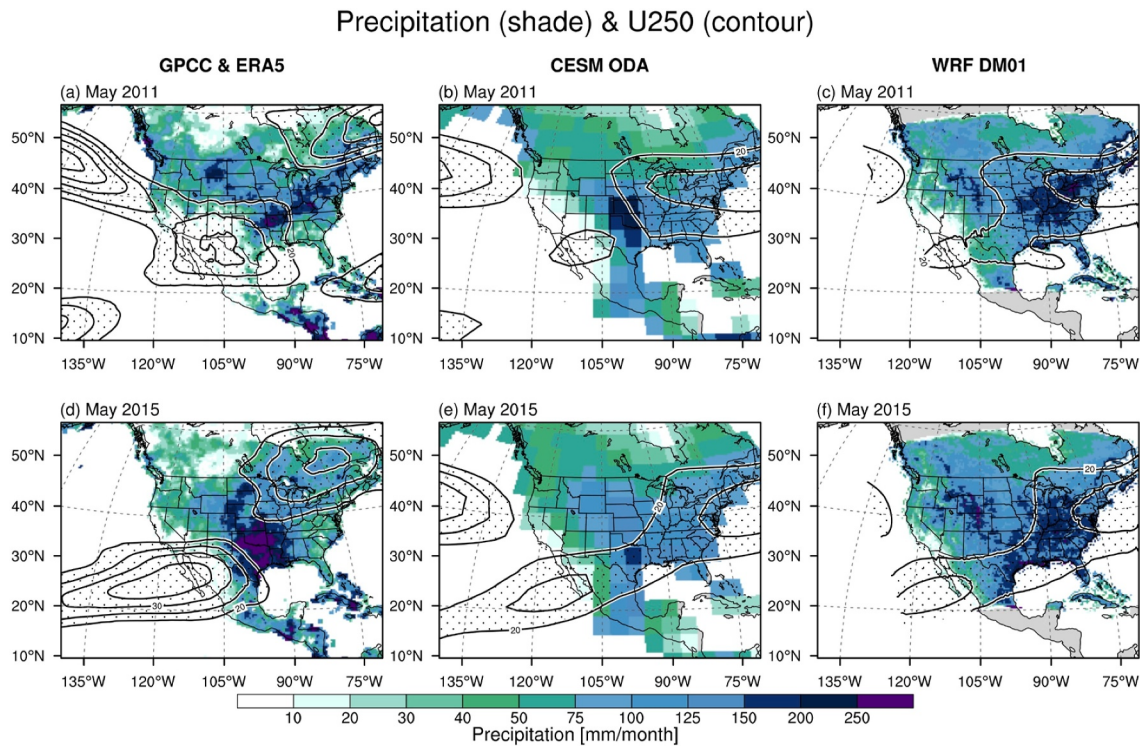


Figure 7. Land precipitation (shaded; mm/month) and U250 maps (contour; m/s) of (a), (d) observations (b), (e) CEMS ODA, and (c), (f) WRF-DM1 in May 2011 (top) and May 2015 (bottom panels). CESM ODA and WRF-DM1 correspond to the ensemble mean of 10 members. Contour interval is 5 m/s. The dotted area indicates that the zonal wind speed is larger than 20 m/s.

including Texas. In contrast, in May 2015, the stronger U250 areas followed a general path from Hawaii to Texas, indicating an active subtropical jet (Figure 7d), which helped transport moist air to the Southern Plains, increasing the chance of high precipitation events. The ensemble mean of CESM ODA tends to capture the strengthened subtropical jet in May 2015, although the model underestimated it as well as the strengthened subpolar jet in May 2011 (Figures 7b and 7e). These model deficiencies make it challenging to simulate the amplitude and spatial extent of precipitation extremes around Texas in the coarse resolution model (Figures 7b and 7e). The WRF-DM1 simulation demonstrates a similar U250 pattern with the CESM ODA but offers a better representation of precipitation in Texas (Figures 7c and 7f). Specifically, both the WRF-DM1 and CESM ODA showed a stronger subtropical jet in May 2015 than in May 2011. The WRF-DM1 simulated heavy precipitation in Texas in May 2015, whereas the CESM ODA significantly underestimated it and hardly resolved the precipitation extremes due to its coarse resolution. These results suggest that precipitation in Texas can be partly attributed to the relative strength between the subtropical and subpolar jets, and a finer horizontal resolution can provide a better representation of the precipitation associated with this large-scale pattern.

The importance of subtropical and subpolar jet activity is also highlighted by comparing individual ensemble members. Figure 8 shows the inter-ensemble correlation maps of precipitation and U250 with the Texas precipitation in CESM ODA and WRF-DM1 simulations. In these maps, anomalies in individual members are defined as the deviation from the ensemble mean for May 2015 or May 2011 months. Therefore, the member simulating higher Texas precipitation generally exhibits positive correlation coefficients from enhanced precipitation or stronger U250 and vice versa. The Texas precipitation is defined by the area average of black box regions in Figures 8a and 8b. The inter-ensemble correlation maps exhibit positive precipitation deviation in the Texas area, negative U250 deviation in Pacific Northwest, and positive U250 deviation in northern Mexico in both CESM ODA and WRF-DM1 simulations (Figure 8). These results indicate that a member having a stronger subtropical jet than the subpolar jet is prone to larger precipitation anomalies in Texas. We can find a similar large-scale pattern of correlation maps between CESM ODA and WRF-DM1 simulations (left vs. right panels in Figure 8). This similarity implies that our dynamical downscaling approach is appropriate for maintaining large-scale features. As shown in Figure 7, however, Texas precipitation simulated by the WRF-DM1 is in better

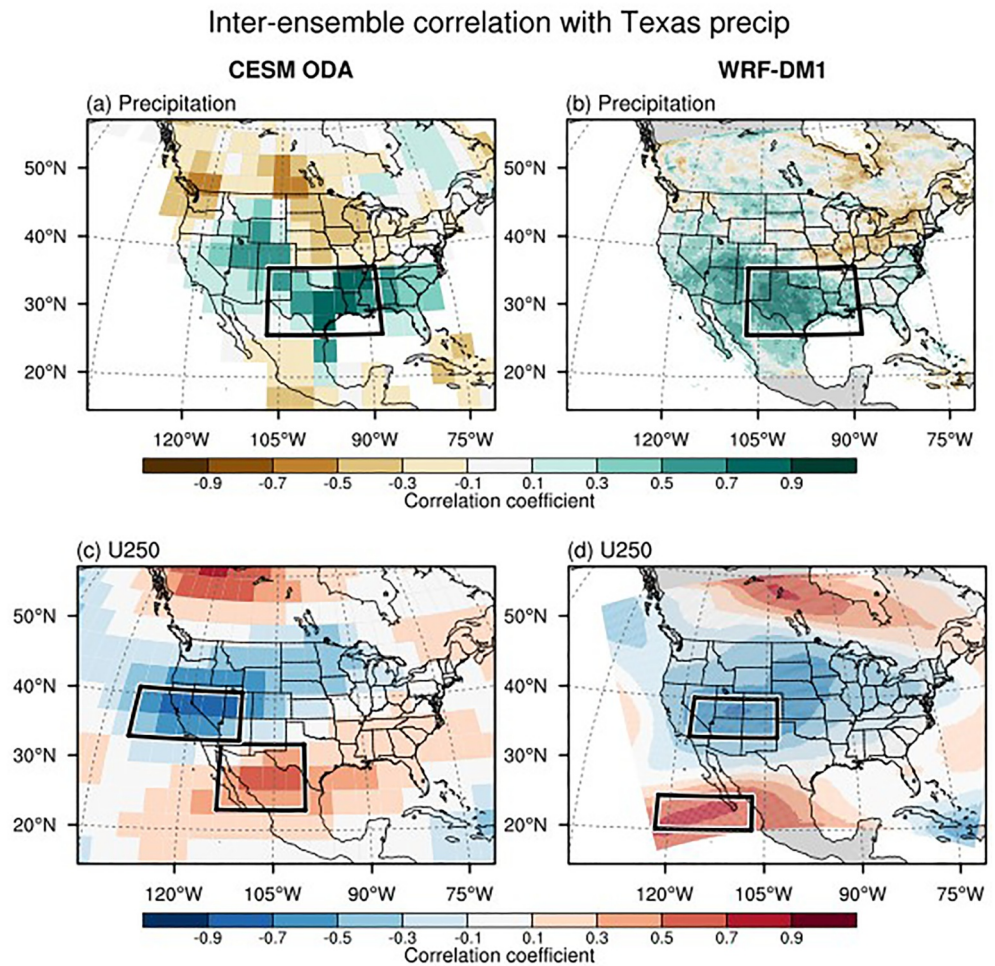


Figure 8. Inter-ensemble correlation of (a), (b) precipitation and (c), (d) U250 anomalies with the area averaged precipitation anomalies (black box in a and b) in the CESM ODA (left) and the WRF-DM1 simulations (right panels). Anomalies are defined as deviations from the ensemble mean at each grid point. The total sampling size is 20 (10 members x 2 case years).

agreement with observations. This better precipitation simulation around the Texas area results in improved simulations for the location and strength of jet stream activity through the dynamical downscaling approach. As a result, we find the shifted locations of the highest correlation coefficients for the U250 deviation between CESM ODA and WRD-DM1 simulations (Figures 8c and 8d).

To quantify the relationship between the jet strengths and precipitation in our area of interest, we made a scatter plot for the Texas precipitation and the difference between a U250 representation of the subtropical and subpolar jets in each ensemble member in May 2011 (blue) and May 2015 (red) in Figure 9. Positive values for this difference indicate that the subtropical jet is stronger than the subpolar jet, favoring more precipitation in Texas through moisture transport. Negative values, meanwhile, indicate that the subpolar jet is stronger, favoring drier conditions in this area. Indeed, the ensemble members with enhanced Texas precipitation show stronger subtropical jets, whereas the members depicting less precipitation show weaker subtropical jets and, overall, this relationship exhibits a high correlation coefficient in both CESM ODA and WRF-DM1 simulations ($R = 0.83$ and $R = 0.77$, respectively). In May 2015, ensemble member #10 demonstrated the most substantial amount of precipitation over Texas and a subtropical jet pattern that is similar to observations (Figures S6j and S7j in Supporting Information S1). In May 2011, ensemble member #6 showed less precipitation around Texas and a strong subpolar jet extending toward the Southwest, which also reflected observations (Figures S4f and S5f in Supporting Information S1). These results support our finding that the relative strength of subtropical and subpolar jets is crucial for better simulation of Texas precipitation. In fact, the ensemble members in the WRF-DM1

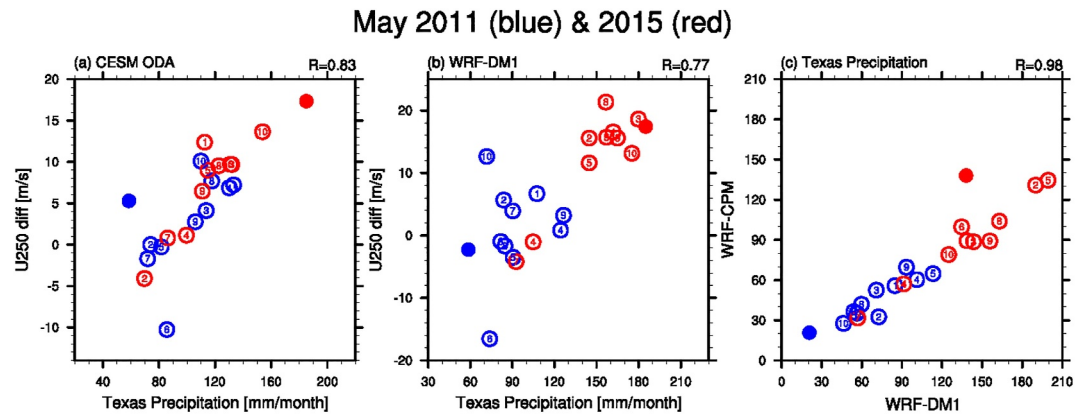


Figure 9. Scatter plots between Texas precipitation (black box in Figures 8a and 8b) and U250 difference (difference in regional averages of the black boxes in Figures 7c and 7d) in each ensemble member and observation for (a) the CESM ODA and (b) the WRF-DM1 simulations. (c) A scatter plot of Texas precipitation averaged in the WRF-CPM domain (i.e., Figure 1) for the WRF-DM1 and WRF-CPM simulations. Blue and red colors indicate May 2011 and May 2015, respectively. The numbers indicate individual ensemble members, and the filled circles are observations. A correlation coefficient is denoted in the upper-right corner. A correlation coefficient greater than 0.40 is statistically significant at the 99.9% level with 38 degrees of freedom.

simulation were tightly distributed around the observations (Figure 9b), except for ensemble members #4 and #7 in May 2015, whereas the ensemble members in the CESM ODA simulation scattered widely compared to the WRF-DM1 simulations (Figure 9a). Under the same subtropical jet influence, precipitation during the extreme convective season is significantly better simulated by WRF-DM1 (red circles, Figure 9b) than CESM ODA (red circles, Figure 9a). Additionally, there is consistency in ensemble spread for the monthly mean Texas precipitation between WRF-DM1 and WRF-CPM members (Figure 9c). Since the WRF-CPM covers the small domain around Texas only, the improved synoptic-scale simulation of jet stream activity (i.e., positions and intensities) in WRF-DM1 leads to a more accurate depiction of precipitation characteristics in Texas and enhances the fidelity of WRF-CPM simulations.

4. Conclusions and Discussion

This study demonstrates the utility of the dynamic downscaling of CPM regional climate modeling data in service to the ocean assimilation of CESM data for the purpose of capturing two extreme rainy seasons, the drought onset of May 2011 and the flooding of May 2015.

Utilizing the coarse resolution in CESM ODA offers a significant advantage in terms of computational efficiency. Doubling the horizontal resolution requires approximately 10 times more computational resources, taking into account factors such as longitude, latitude, height, and time resolutions. By employing the coarse horizontal resolution of CESM, we can effectively allocate the remaining computational resources to better account for statistical and physical uncertainty in a modeling system, including the execution of regional models like WRF and CPM, the augmentation of ensemble size, and the incorporation of additional Earth system components (e.g., atmospheric chemistry, sophisticated hydrology, crop models, dynamical vegetation, river modules, land ice modeling, global carbon cycle, and marine ecosystems). This allocation also allows for an increase in the number of vertical layers, enabling the resolution of the stratosphere and mesosphere, as well as the advancement of data assimilation schemes (e.g., 4DVAR and EnKF). Our approach in using CESM ODA can also provide reasonable initial conditions for conducting hindcast and forecast runs, as demonstrated in previous work (Chikamoto et al., 2019, 2020b). This approach can be combined with the dynamical downscaling of CPM. This presents a significant advantage compared to AMIP-type experiments, which cannot be used for future climate forecasting due to the absence of forecasted sea surface temperatures (SST). Introducing a higher atmospheric resolution in CESM (e.g., T42 or T85) would only marginally facilitate the dynamical downscaling process, by reducing the resolution gap between the global and regional models. However, it is more essential, in our view, to consider various other factors that impact the performance of climate models, such as coupler processes, mean state biases,

and ocean data assimilation techniques, as they contribute to model diversity. Our findings demonstrate that the application of dynamical downscaling allows us to overcome the limitations of lower horizontal resolution, thereby improving simulations of extreme precipitation events over a specific area of interest. Our results also hold significant implications for the application of recently developed unstructured grids, such as the Voronoi mesh (Skamarock et al., 2012) and the spectral element dynamical core (Zarzycki et al., 2015). These dynamical cores enable the use of variable resolutions within AGCMs. Our successful demonstration of dynamical downscaling, when combined with the low-resolution CESM, supports the feasibility of employing variable mesh resolutions. For example, this could involve lower resolutions over the ocean, higher resolutions in the United States, and cloud-permitted resolutions for regions like Texas.

CESM ODA ensembles have either very low or no skill in capturing the convective extreme events in May 2015, and the no-rain climatology in May 2011 is also not consistently simulated. As mentioned in the introduction, it is generally known that dynamical downscaling the coarser resolution climate models with CPM resolution can reduce key uncertainties in the representation of precipitation, thus improving the depiction of convective precipitation in regional climate models with respect to timing, duration, and intensity. When using CPM-type dynamical downscaling to seasonal or longer-term predictions provided by global climate models (GCMs), the resulting forecast skill is highly dependent on the biases of the driving GCMs. It is also unclear how much the results produced by CPM came from the coarser resolution forcing versus from the CPM. Our results suggest that an improved regional circulation pattern depiction, as obtained from the partial data assimilation, combined with CPM, can lead to improved precipitation simulations.

The CPM ensemble simulations indicate consistent improvements in the depiction of precipitation that matches observations not only for extreme rainfall thresholds and the distribution of precipitation in the wet spring of May 2015, but also for the overall precipitation pattern in the drought-onset spring of May 2011. It also results in much improved convection-related simulated precipitation at the meso- α (CESM, 100s km) and meso- β (WRF-DM1, 10s km) resolutions to meso- γ (CPM, <5 km) resolution. For minimal to moderate rainfall amounts below 50 mm, CESM ODA and CPM have similar modeling capability. CESM ODA fails to capture precipitation extremes exceeding 100 mm, a shortcoming that is improved by CPM dynamical downscaling. The strength of the CPM, it appears, is its ability to capture extreme precipitation if the large-scale circulation features are more skillfully represented within the driving global model.

Our analyses found that different sources of upper atmospheric zonal winds may lead to abnormally wet or dry seasonal precipitation in Texas. Strong subtropical jets provide the constant source of moisture that can support robust convective precipitation, creating the conditions for floods in the Southern Plains, while subpolar jets lead to dry atmospheric conditions and thus potential drought.

Preexisting soil and atmospheric conditions will always play a role in prolonged wet and dry periods (for instance, by some estimates, the Texas dry spell started in the summer of 2010, a year before the abnormally dry month we examined) and these factors are important to note, albeit beyond the scope of the objectives in this manuscript. Whatever the antecedent conditions may have been, however, it is clear that the aberrantly dry May 2011 substantially contributed to Texas' worst drought period since 1895 (Yoon et al., 2018). Likewise, while preexisting soil saturation may have contributed to the flooding in May 2015, that event was clearly a result of consistent, higher-than-normal precipitation in that month and the months leading up to it. These two events may thus serve as a guide for further examination of the ways in which the CESM ODA may be employed to extend the simulation lead time for significant pluvial and drought conditions in the Southern Plains and potentially elsewhere in the Western United States (Chikamoto, Johnson, et al., 2020).

Our results also demonstrate the critical implications for sub-seasonal-to-seasonal forecasts. The CESM ODA used in this study can provide the initial conditions to conduct hindcast and forecast experiments based on the CESM free run. Even though the forecasted product in CESM can simulate only the large-scale features driven mainly by the ocean forcing and cannot resolve the mesoscale precipitations, the WRF dynamical downscaling approach introduced here could improve the model performance in simulating regional-scale precipitation extremes. The outcomes of these products could provide valuable information to stakeholders and policymakers to manage extreme weather hazards.

Data Availability Statement

All relevant data used in this manuscript are available on institutional data repository. CESM ODA ensembles and post-processed WRF-CPM ensembles are available on the University of Arizona Research Data Repository. Post-processed Weather Research and Forecasting model and Community Earth System Model data sets (Dataset, Chang et al., 2023a), <https://doi.org/10.25422/azu.data.23820741.v1>. Statistical analysis coding templates (Software, Chang et al., 2023b), <https://doi.org/10.25422/azu.data.23820672.v1>.

Acknowledgments

This work is supported by the following grants: U.S. Department of Defense, Strategic Environmental Research and Development Program (SERDP, RC20-3056); U.S. Department of Interior, Bureau of Reclamation (R19AP00149 and R22AP00220), U.S. Department of Energy grant (DESC0016605); Utah State University, Utah Agricultural Experiment Station.

References

- Balmaseda, M. A., Mogens, K., & Weaver, A. T. (2013). Evaluation of the ECMWF ocean reanalysis system ORAS4. *Quarterly Journal of the Royal Meteorological Society*, *139*(674), 1132–1161. <https://doi.org/10.1002/qj.2063>
- Bloom, S. C., Takacs, L. L., Da Silva, A. M., & Ledvina, D. (1996). Data assimilation using incremental analysis updates. *Monthly Weather Review*, *124*(6), 1256–1271. [https://doi.org/10.1175/1520-0493\(1996\)124<1256:dauiuu>2.0.co;2](https://doi.org/10.1175/1520-0493(1996)124<1256:dauiuu>2.0.co;2)
- Bukovsky, M. S., & Karoly, D. J. (2011). A regional modeling study of climate change impacts on warm-season precipitation in the Central United States. *Journal of Climate*, *24*(7), 1985–2002. <https://doi.org/10.1175/2010jcli3447.1>
- Capecchi, V. (2021). Reforecasting two heavy-precipitation events with three convection-permitting ensembles. *Weather and Forecasting*, *36*(3), 769–790. <https://doi.org/10.1175/WAF-D-20-0130.1>
- Castro, C. L., Chang, H.-I., Dominguez, F., Carrillo, C., Kyung-Schemm, J., & Juang, H. H.-M. (2012). Can a regional climate model improve warm season forecasts in North America? *Journal of Climate*, *25*(23), 8212–8237. <https://doi.org/10.1175/jcli-d-11-00441.1>
- Chang, H.-I., Castro, C. L., Carrillo, C., & Dominguez, F. (2015). The more extreme nature of U.S. warm season climate in the recent observational record and two “well performing” dynamically downscaled CMIP3 models. *Journal of Geophysical Research*, *120*(16), 8244–8263. <https://doi.org/10.1002/2015jd023333>
- Chang, H.-I., Yoshimitsu, C., & Risanto, C. B. (2023a). Post-processed weather Research and forecasting model and community Earth system model datasets to understand extreme Texas drought and flood years [Dataset]. *University of Arizona Research Data Repository*. <https://doi.org/10.25422/azu.data.23820741.v1>
- Chang, H.-I., Yoshimitsu, C. B., & Risanto, C. (2023b). Statistical analysis templates for the weather Research and forecasting model and community Earth system model [Software]. *University of Arizona Research Data Repository*, <https://doi.org/10.25422/azu.data.23820672.v1>
- Chikamoto, Y., Johnson, Z. F., Wang, S.-Y. S., McPhaden, M. J., & Mochizuki, T. (2020). El Niño–Southern oscillation evolution modulated by Atlantic forcing. *Journal of Geophysical Research Oceans*, *125*(8), e2020JC016318. <https://doi.org/10.1029/2020jc016318>
- Chikamoto, Y., Timmermann, A., Widlansky, M. J., Zhang, S., & Balmaseda, M. A. (2019). A drift-free decadal climate prediction system for the Community Earth System Model. *Journal of Climate*, *32*(18), 5967–5995. <https://doi.org/10.1175/JCLI-D-18-0788.1>
- Chikamoto, Y., Timmermann, A., Widlansky, M. J., Zhang, S., Balmaseda, M. A., & Stott, L. (2017). Multi-year predictability of climate, drought, and wildfire in southwestern North America. *Scientific Reports*, *7*(1), 6568. <https://doi.org/10.1038/s41598-017-06869-7>
- Chikamoto, Y., Wang, S.-Y. S., Yost, M., Yocom, L., & Gillies, R. R. (2020b). Colorado River water supply is predictable on multi-year timescales owing to long-term ocean memory. *Communications Earth & Environment*, *1*, 26. <https://doi.org/10.1038/s43247-020-00027-0>
- Coumou, D., Petoukhov, V., Rahmstorf, S., Petri, S., & Schellnguber, H. J. (2014). Quasi-resonant circulation regimes and hemispheric synchronization of extreme weather in boreal summer. *Proceedings of the National Academy of Sciences of the United States of America*, *139*(674), 1132–1161. <https://doi.org/10.1073/pnas.1412797111>
- Croci-Maspoli, M., Schwierz, C., & Davies, H. (2007). A multi-faceted climatology of atmospheric blocking and its recent linear trend. *Journal of Climate*, *20*(4), 633–649. <https://doi.org/10.1175/jcli4029.1>
- Diallo, I., Xue, Y., Li, Q., De Sales, F., & Li, W. (2019). Dynamical downscaling the impact of spring western US land surface temperature on the 2015 flood extremes at the southern Great plains: Effect of domain choice, dynamic cores and land surface parameterization. *Climate Dynamics*, *53*(1–2), 1039–1061. <https://doi.org/10.1007/s00382-019-04630-6>
- Fosser, G., Kendon, E. J., Stephenson, D., & Tucker, S. (2020). Convection-permitting models offer promise of more certain extreme rainfall projections. *Geophysical Research Letters*, *47*(13), e2020GL088151. <https://doi.org/10.1029/2020GL088151>
- Francis, J. A., & Vavrus, S. J. (2012). Evidence linking Arctic amplification to extreme weather in mid-latitudes. *Geophysical Research Letters*, *39*(6). <https://doi.org/10.1029/2012GL051000>
- Ghebreyesus, D., & Sharif, H. O. (2021). Time series analysis of monthly and annual precipitation in the state of Texas using high-resolution radar products. *Water*, *13*(7), 982. <https://doi.org/10.3390/w13070982>
- Harvey, L. O., Hammond, K. R., Lush, C. M., & Mross, E. F. (1992). The application of signal detection theory to weather forecasting behavior. *Monthly Weather Review*, *120*(5), 863–883. [https://doi.org/10.1175/1520-0493\(1992\)120<0863:taostd>2.0.co;2](https://doi.org/10.1175/1520-0493(1992)120<0863:taostd>2.0.co;2)
- Higgins, R. W., Yao, Y., Yarosh, E. S., Janowiak, J. E., & Mo, K.-C. (1997). Influence of the Great Plains lowlevel jet on summertime precipitation and moisture transport over the central United States. *Journal of Climate*, *10*(3), 481–507. [https://doi.org/10.1175/1520-0442\(1997\)010<0481:iotgpl>2.0.co;2](https://doi.org/10.1175/1520-0442(1997)010<0481:iotgpl>2.0.co;2)
- Holloway, C. E., & Neelin, J. D. (2009). Moisture vertical structure, column water vapor, and tropical deep convection. *Journal of the Atmospheric Sciences*, *66*(6), 1665–1683. <https://doi.org/10.1175/2008jas2806.1>
- Huang, B., Kinter, J., & Schopf, P. (2002). Ocean data assimilation using intermittent analyses and continuous model error correction. *Advances in Atmospheric Sciences*, *19*(6), 965–992. <https://doi.org/10.1007/s00376-002-0059-z>
- Johnson, Z. F., Chikamoto, Y., Luo, J.-J., & Mochizuki, T. (2018). Ocean impacts on Australian interannual to decadal precipitation variability. *Climate*, *6*(3), 61. <https://doi.org/10.3390/cli6030061>
- Johnson, Z. F., Chikamoto, Y., Wang, S. Y. S., McPhaden, M. J., & Mochizuki, T. (2020). Pacific decadal oscillation remotely forced by the equatorial Pacific and the Atlantic Oceans. *Climate Dynamics*, *55*(3–4), 789–811. <https://doi.org/10.1007/s00382-020-05295-2>
- Karmalkar, A. V., Bradley, R. S., & Diaz, H. F. (2011). Climate change in Central America and Mexico: Regional climate model validation and climate change projections. *Climate Dynamics*, *37*(3–4), 605–629. <https://doi.org/10.1007/s00382-011-1099-9>
- Kelly, D. L., Schaefer, J. T., McNulty, R. P., Doswell, III, C. A., & Abbey, R. F., Jr. (1978). An augmented tornado climatology. *Monthly Weather Review*, *106*(8), 1172–1183. [https://doi.org/10.1175/1520-0493\(1978\)106<1172:aatc>2.0.co;2](https://doi.org/10.1175/1520-0493(1978)106<1172:aatc>2.0.co;2)

- Kendon, E. J., Ban, N., Roberts, N. M., Fowler, H. J., Roberts, M. J., Chan, S. C., et al. (2017). Do convection-permitting regional climate models improve projections of future precipitation change. *Bulletin of the American Meteorological Society*, 98(1), 79–93. <https://doi.org/10.1175/BAMS-D-15-0004.1>
- Lee, S.-K., Mapes, B. E., Wang, C., Enfield, D. B., & Weaver, S. J. (2014). Springtime ENSO phase evolution and its relation to rainfall in the continental U.S. *Geophysical Research Letters*, 41(5), 1673–1680. <https://doi.org/10.1002/2013GL059137>
- Lin, Y., & Mitchell, K. E. (2005). 1.2 The NCEP stage II/IV hourly precipitation analyses: Development and applications (Vol. 10). *Proceedings of the 19th conference hydrology American meteorological society*.
- Luong, T. M., Castro, C. L., Chang, H.-I., Lahmers, T., Adams, D. K., & Ochoa-Moya, C. A. (2017). The more extreme nature of North American monsoon precipitation in the southwestern U.S. As revealed by a historical climatology of simulated severe weather events. *Journal of Applied Meteorology and Climatology*, 56(9), 2509–2529. <https://doi.org/10.1175/jamc-d-16-0358.1>
- Meredith, E. P., Maraun, D., Semenov, V. A., & Park, W. (2015). Evidence for added value of convection-permitting models for studying changes in extreme precipitation. *Journal of Geophysical Research: Atmospheres*, 120, 12500–12513. <https://doi.org/10.1002/2015JD024238>
- Nielsen, E. R., & Schumacher, R. S. (2016). Using convection-allowing ensembles to understand the predictability of an extreme rainfall event. *Monthly Weather Review*, 144(10), 3651–3676. <https://doi.org/10.1175/MWR-D-16-0083.1>
- Nigam, S., & Ruiz-Barradas, A. (2006). Seasonal hydroclimate variability over North America in global and regional reanalyses and AMIP simulations: Varied representation. *Journal of Climate*, 19(5), 815–837. <https://doi.org/10.1175/jcli3635.1>
- Powers, J. G., Klemp, J. B., Skamarock, W. C., Davis, C. A., Dudhia, J., Gill, D. O., et al. (2017). The weather Research and forecasting (WRF) model: 575 overview, system efforts, and future directions. *Bulletin of the American Meteorological Society*, 98(8), 1717–1737. <https://doi.org/10.1175/BAMS-D-15-00308.1>
- Prein, A. F., Langhans, W., Fossler, G., Ferrone, A., Ban, N., Goergen, K., et al. (2015). A review on regional convection-permitting climate modelling: Demonstrations, prospects, and challenges: Convection-permitting climate modelling. *Review of Geophysics*, 53(2), 323–361. <https://doi.org/10.1002/2014rg000475>
- Prein, A. F., Rasmussen, R., Castro, C. L., Dai, A., & Minder, J. (2020). Special issue: Advances in convection-permitting climate modeling. *Climate Dynamics*, 55(1–2), 1–2. <https://doi.org/10.1007/s00382-020-05240-3>
- Qing, Y., & Wang, S. (2021). Multi-decadal convection-permitting climate projections for China's Greater Bay Area and surroundings. *Climate Dynamics*, 57(1–2), 415–434. <https://doi.org/10.1007/s00382-021-05716-w>
- Risanto, C. B., Castro, C. L., Moker, J. M., Arellano, A. F., Adams, D. K., Fierro, L. M., & Minjarez Sosa, C. M. (2019). Evaluating forecast skills of moisture from convective-permitting WRF-ARW model during 2017 North American Monsoon season. *Atmosphere*, 10(11), 694. <https://doi.org/10.3390/atmos10110694>
- Roads, J. O., Chen, S.-C., Guetter, A. K., & Georgakakos, K. P. (1994). Large-scale aspects of the United States hydrologic cycle. *Bulletin of the American Meteorological Society*, 75(9), 1589–1610. [https://doi.org/10.1175/1520-0477\(1994\)075<1589:lsaotu>2.0.co;2](https://doi.org/10.1175/1520-0477(1994)075<1589:lsaotu>2.0.co;2)
- Scaff, L., Prein, A. F., Li, Y., Liu, C., Rasmussen, R., & Ikeda, K. (2020). Simulating the convective precipitation diurnal cycle in North America's current and future climate. *Climate Dynamics*, 55(1–2), 369–382. <https://doi.org/10.1007/s00382-019-04754-9>
- Schneider, U., Ziese, M., Meyer-Christoffer, A., Finger, P., Rustemeier, E., & Becker, A. (2017). The new portfolio of global precipitation data products of the Global Precipitation Climatology Centre suitable to assess and quantify the global water cycle and resources. *Proc. IAHS*, 374, 29–34. <https://doi.org/10.5194/piahs-374-29-2016>
- Schubert, S., Wang, H., & Suarez, M. (2011). Warm season subseasonal variability and climate extremes in the Northern Hemisphere: The role of stationary Rossby waves. *Journal of Climate*, 24(18), 4773–4792. <https://doi.org/10.1175/jcli-d-10-05035.1>
- Screen, J. A., & Simmonds, I. (2013). Exploring links between Arctic amplification and mid-latitude weather. *Geophysical Research Letters*, 40(5), 959–964. <https://doi.org/10.1002/grl.50174>
- Shields, C. A., Bailey, D. A., Danabasoglu, G., Jochum, M., Kiehl, J. T., Levis, S., & Park, S. (2012). The low-resolution CCSM4. *Journal of Climate*, 25(12), 3993–4014. <https://doi.org/10.1175/JCLI-D-11-00260.1>
- Skamarock, W. C., Klemp, J. B., Duda, M. G., Fowler, L. D., Park, S. H., & Ringler, T. D. (2008). A description of the Advanced Research WRF version 3. *NCAR Tech. Note NCAR/TN-475+STR*, 113.
- Skamarock, W. C., Klemp, J. B., Duda, M. G., Fowler, L. D., Park, S. H., & Ringler, T. D. (2012). A multiscale nonhydrostatic atmospheric model using centroidal Voronoi tessellations and C-grid staggering. *Monthly Weather Review*, 140(9), 3090–3105. <https://doi.org/10.1175/MWR-D-11-00215.1>
- Stuivenvolt-Allen, J., Wang, S.-Y. S., Johnson, Z., & Chikamoto, Y. (2021). Atmospheric rivers impacting northern California exhibit a quasi-decadal frequency. *Journal of Geophysical Research Atmosphere*, 126(15), e2020JD034196. <https://doi.org/10.1029/2020JD034196>
- Sun, Q., Miao, C., Duan, Q., Ashouri, H., Sorooshian, S., & Hsu, K.-L. (2018). A review of global precipitation datasets: Data sources, estimation, and intercomparisons. *Reviews of Geophysics*, 56(1), 79–107. <https://doi.org/10.1002/2017rg000574>
- Sun, X., Xue, M., Brotzge, J., McPherson, R. A., Hu, X., & Yang, X. (2016). An evaluation of dynamical downscaling of central plains summer precipitation using a WRF-based regional climate model at a convection-permitting 4 km resolution. *Journal of Geophysical Research-Atmosphere*, 121(23), 13801–13825. <https://doi.org/10.1002/2016JD024796>
- Sun, Y., Riva, R., & Ditmar, P. (2016). Optimizing estimates of annual variations and trends in geocenter motion and J2 from a combination of GRACE data and geophysical models. *Journal of Geophysical Research Solid Earth*, 121(11), 8352–8370. <https://doi.org/10.1002/2016JB013073>
- Trenberth, K. E. (2011). Changes in precipitation with climate change. *Climate Research*, 47(1), 123–138. <https://doi.org/10.3354/cr00953>
- Vanden Broucke, S., Wouters, H., Demuzere, M., & Lipzig, N. P. M. (2019). The influence of convection-permitting regional climate modeling on future projections of extreme precipitation: Dependency on topography and timescale. *Climate Dynamics*, 52(9–10), 5303–5324. <https://doi.org/10.1007/s00382-018-4454-2>
- Wang, S., & Chen, T. (2009). The late-spring maximum of rainfall over the U.S. central plains and the role of the low-level jet. *Journal of Climate*, 22(17), 4696–4709. <https://doi.org/10.1175/2009JCLI2179.1>
- Wang, S.-Y., Davies, R. E., & Gillies, R. R. (2013). Identification of extreme precipitation threat across midlatitude regions based on short-wave circulations. *Journal of Geophysical Research Atmosphere*, 118(11), 11059–11074. <https://doi.org/10.1002/jgrd.50841>
- Wang, S.-Y., Hakala, K., Gillies, R. R., & Capehart, W. J. (2014). The Pacific quasi-decadal oscillation (QDO): An important precursor toward anticipating major flood events in the Missouri River Basin? *Geophysical Research Letters*, 41(3), 2013GL059042. <https://doi.org/10.1002/2013gl059042>
- Wang, S.-Y., Huang, W.-R., Hsu, H.-H., & Gillies, R. R. (2015). Role of the strengthened El Niño teleconnection in the may 2015 floods over the southern Great plains. *Geophysical Research Letters*, 42(19), 8140–8146. <https://doi.org/10.1002/2015gl065211>

- Wilks, D. (2006). *Statistical methods in the atmospheric sciences* (2nd ed., p. 627). Academic Press.
- Yoon, J.-H., & Leung, L. R. (2015). Assessing the relative influence of surface soil moisture and ENSO SST on precipitation predictability over the contiguous United States. *Geophysical Research Letters*, *42*(12), 5005–5013. <https://doi.org/10.1002/2015gl064139>
- Yoon, J.-H., Wang, S. Y. S., Lo, M.-H., & Wu, W.-Y. (2018). Concurrent increases in wet and dry extremes projected in Texas and combined effects on groundwater. *Environmental Research Letters*, *13*(5), 054002. <https://doi.org/10.1088/1748-9326/aab96b>
- Zarzycki, C. M., Jablonowski, C., Thatcher, D. R., & Taylor, M. A. (2015). Effects of localized grid refinement on the general circulation and climatology in the community atmosphere model. *Journal of Climate*, *28*(7), 2777–2803. <https://doi.org/10.1175/JCLI-D-14-00599.1>